processes

MDPI

Article

Simulation and Experimental Study on Vibrating Screen-Type Grain-Recovery Device with Upper Centrifugal Fan

Yanjun Li [1], Yanguang Gong [2], Yongtao Yu [1] and Fuxiang Xie [1,*]

[1] School of Machinery and Automation, Weifang University, Weifang 261000, China; liyanjun@wfu.edu.cn (Y.L.); 20210085@wfu.edu.cn (Y.Y.)
[2] Honeywell Environment & Combustion Controls (Tianjin) Co., Ltd., Tianjin 300457, China; 20210025@wfu.edu.cn
* Correspondence: xfx608@wfu.edu.cn; Tel.: +86-177-0636-5915

Abstract: To solve the problem of grain loss caused by nibbling during the working process of the maize ear and stem harvesting machine, a vibrating screen-type grain-recovery device with an upper centrifugal fan was designed. The device mainly consists of a centrifugal fan and vibrating screen. The work process of the grain-recovery device is theoretically analyzed, and it is clarified that the turning of the bracts is the key to separating the bracts from the grains, and the design criteria of the vibrating screen are obtained. The CFD–EDEM coupled single-factor simulation experiment was carried out on the size of the vibrating screen sieve hole and the number of draft bars, and the motion posture of the bracts was simulated. Based on the previous CFD–EDEM coupled simulation study, the orthogonal experiment was carried out on the fan speed, vibration screen drive-shaft speed, and operation speed of the grain-recovery device. The orthogonal experimental results show that, when the fan speed is 1000 r/min, the vibration screen drive-shaft speed is 300 r/min, and the operation speed is 3.62 km/h, the performance of the grain-recovery device reaches the optimum level, and the grain recovery rate is approximately 85%.

Keywords: grain recovery; CFD–EDEM; orthogonal experiment; virtual simulation

Citation: Li, Y.; Gong, Y.; Yu, Y.; Xie, F. Simulation and Experimental Study on Vibrating Screen-Type Grain-Recovery Device with Upper Centrifugal Fan. *Processes* **2023**, *11*, 2654. https://doi.org/10.3390/pr11092654

Academic Editor: Andrew Hoadley

Received: 11 August 2023
Revised: 28 August 2023
Accepted: 2 September 2023
Published: 5 September 2023

1. Introduction

Currently, corn grain-recovery devices in the world can be mainly divided into three types: scraper, auger, and vibrating screen [1,2]. The scraper equipment separates the remaining husks and grains after corn peeling for recovery [3]. The chain scraper sends the husks outside the machine, while the grains are separated through sieve holes. However, this method struggles to separate the grains trapped in the husks, resulting in significant losses [4]. The auger recovery device is simple, low-cost, durable, and safe, but it does not generate vibrations during the recovery process [5]. Therefore, it is difficult to separate corn grains in the presence of husks and other impurities, leading to low recovery rates and the machine being easily affected by blockages caused by impurities [6]. The vibrating screen recovery device separates grains from husks through vibration and is less prone to impurity accumulation. However, it is also challenging to separate corn grains trapped within the husks.

Currently, there are two main methods of corn harvesting in Europe and America. One is the direct harvesting of corn grains. In countries like the United States and Germany, where corn cultivation is mostly performed once a year and the grain moisture content is low during harvest, the direct grain harvesting method is widely used. During corn harvesting, it is only necessary to replace the grain header on the grain combine harvester and adjust the speed of the threshing drum and the threshing clearance for corn harvesting. The representative model is John Deere's X9 combine harvester (Figure 1) [3]. And to address the issue of the high grain-breakage rate during direct harvesting of corn grains, large agricultural machinery companies, such as John Deere, CASE, New Holland, and

CLAAS, have installed real-time performance monitoring and operation parameter self-adjustment systems on their harvesters [7]. The other method is ear harvesting. In Eastern European countries like Ukraine where the moisture content of the ears is higher during harvest, the method of harvesting ears, including husk removal and grain collection, is used. Some models are equipped with stalk shredders for integrated ear-stalk harvesting. The KCKY-6 maize combine harvester (Figure 2) produced by the former Soviet Union is the only representative example of a device with grain-recovery functionality [8]. It uses a scraper-type grain-recovery device consisting of circular sieve plates and chain scrapers. The rotating scraper sends the corn husks out of the machine, while the corn grains are separated through sieve holes and slide into the ear conveyor for convenient recovery. However, due to the difficulty of separating grains trapped in the husks, the grain-recovery rate is not high, and it has not been widely used in China [9]. In contrast, China mainly adopts auger and vibrating screen grain-recovery devices. However, due to the challenging separation of grains trapped in the husks, grain losses occur. Hence, many domestic experts and scholars have conducted extensive research and exploration on this issue. Wang Gaobin designed a segmented vibrating screen grain-recovery device that can crush the corn stalks and husks that fall during peeling, causing the corn grains trapped in the husks to fall out, thereby improving the grain-recovery rate. The scheme achieved optimization through theoretical analysis and field experiments, resulting in a 15.28% increase in the grain-recovery rate [10]. Zhou Xiaohui et al. integrated the husk crushing device with the grain-recovery device using the auger to push the husks and grains, separating them through a screening mesh. The separated grains and lightweight impurities are further separated and recovered under the action of wind, while the husks are transported to the cutting box for shredding, enabling the recovery of grains and serving as fertilizer for returning to the field [11]. Jing Yi designed and developed an auger-type grain-recovery device, which separates grains and impurities by agitating the material through a grain stirrer and then uses an auger conveying device to recover the grains [12].

Figure 1. John Deere's X9 combine harvester.

Based on the above analysis, the key to grain-recovery devices in maize stalk and ear combine harvesters is to separate the grains trapped in the husks. Many experts and scholars have conducted extensive research on this matter using methods such as husk crushing, augers, and scrapers to separate the husks from the grains. Compared with this device, the structure of the upward-mounted fan vibrating screen grain-recovery device that we designed is simpler. The impurity content in the recovered grains is reduced because the bracts are expelled from the body instead of being crushed, and the recovery efficiency is higher because of the reasonable structure [13–15]. Through theoretical analysis and CFD–EDEM coupled simulation, it was demonstrated that the device can change the posture of the husks and optimize the structure of the vibrating screen. Field orthogonal experiments were conducted on the optimized grain-recovery device, resulting in the determination of its optimal working parameters. This research provides a theoretical basis

for the design of grain-recovery devices in maize stalk and ear combine harvesters and holds promise for engineering applications.

Figure 2. KCKY-6 maize combine harvester.

The overview structure of this paper is shown in Figure 3.

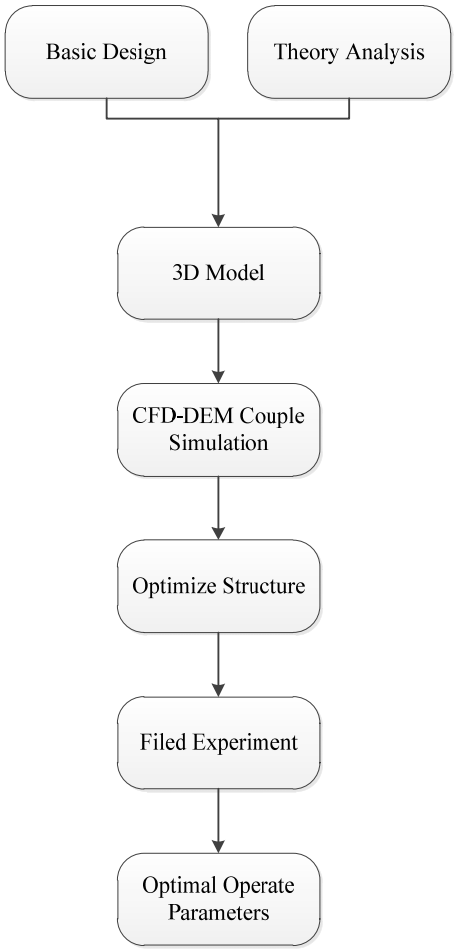

Figure 3. The structure of the paper.

2. Structure and Working Principle of the Top-Mounted Fan Vibrating Screen Grain-Recovery Device

The upward-mounted fan vibrating screen grain-recovery device consists of a frame, centrifugal fan, driving device, vibrating screen, front slide plate, and rear slide plate (Figure 4). The frame is divided into two parts: the peeling device bracket and the recovery chamber bracket. The peeling device bracket has four slide plates (front, rear, left, and right) to guide the mixture of husks, leaves, short stalks, and grains peeled off by the peeling device into the recovery chamber. Under the influence of the airflow, the husks flip over, causing the grains to fall and separate. Some husks and leaves are blown outside the machine by the airflow, while the remaining husks, short stalks, and corn grains fall onto the screening surface of the vibrating screen. The vibrating screen is designed with a negative angle and equipped with raking bars for better material separation. It also allows for the husks and short stalks to be discharged outside the machine. The driving device consists of a main shaft, eccentric small shaft, connecting rod, swing rod, screen shaft, pivot shaft, and small shaft, which are used to drive the vibration of the vibrating screen. The swing rod connects with the screen shaft and pivot shaft, causing the front end of the vibrating screen to oscillate back and forth, while the rear end of the screen is equipped with a slide rail for sliding on the small shaft bearing. This device reduces the impurity content in the recovered material and improves the grain-recovery rate.

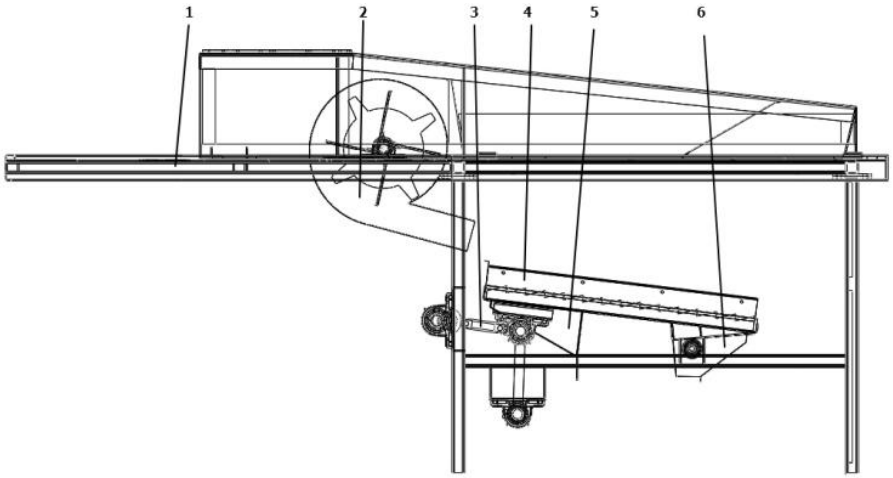

Figure 4. Corn Recycling Device with Vibrating Screen and Fan on Top. 1—frame; 2—centrifugal fan; 3—driving device; 4—vibrating screen; 5—vibrating screen before the slide; 6—vibrating screen after the slide.

2.1. Design and Analysis of Key Components

Unlike grain-recovery devices for crops such as wheat, corn grain-recovery devices primarily recover the residual grains trapped in the corn husks and require the separation of the husks and grains through the action of airflow and vibrating screens [16]. Therefore, when designing grain-recovery devices, it is crucial to focus on the analysis of the forces exerted on the materials during airflow and the design of the vibrating screen.

2.1.1. Design of the Fan and Analysis of the Force Exerted on the Material in the Airflow Field

The main function of the fan in this device is to induce the flipping of the husks and separate the grains trapped in the husks. To achieve this goal, a higher outlet wind speed is required [17]. However, the recovery chamber is relatively short, leading to rapid decay of the wind speed [18]. Therefore, a low-pressure, medium-speed centrifugal fan is chosen. To maintain uniform wind speed, especially when the fan diameter is small, measures such as using four straight blades and trimming a triangular block from the fan blades are adopted

to increase the incoming air volume in the middle and facilitate air entry from both sides of the fan, as shown in Figure 5.

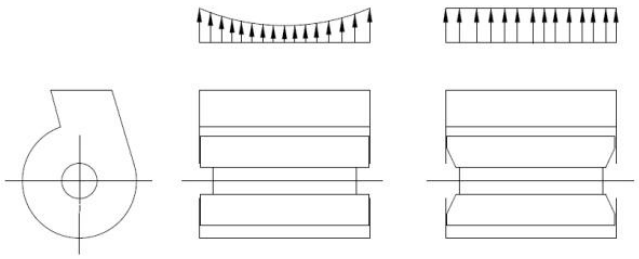

Figure 5. The distribution of outlet flow velocity of the wind turbine in the width direction.

The bracts are directly affected by the airflow blown out from the fan in the sorting room. To verify whether the arrangement of the fan can achieve the effect of separating the bracts from the seeds, it is necessary to analyze the forces and motion of the bracts in the airflow field [19,20]. The instantaneous force situation of the bracts entering the airflow field is shown in Figure 6.

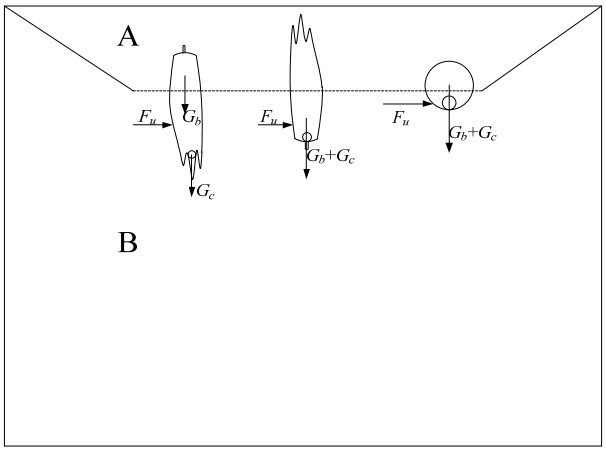

Figure 6. The force situation of the involucral leaves at the moment of entering the airflow field.

For ease of analysis, it is assumed that there is no airflow in the upper space of the slide plate (Area A in the diagram) and that the bracts only experience the airflow when they fall into the lower space of the slide plate (Area B in the diagram). From observations of the bracts falling from the defoliator and sliding plate, there are three typical orientations: stem up, stem down, and horizontal fall [21–23]. To analyze the motion of the bracts, it is necessary to analyze the forces acting on each of these three initial orientations.

The force analysis shows that the bracts are mainly subjected to the forces of airflow F_u, the gravity of the bracts G_b, and the gravity of the corn G_c in the airflow field. Due to different initial postures, the points of action for these three forces are also different.

The force analysis indicates that the bracts in the airflow field are mainly influenced by the airflow force, the weight of the bracts, and the weight of the seeds. Due to the different points of application for these three forces, the following three scenarios exist. (1) When the initial orientation is stem up, due to the force of gravity, the seeds will gather at the bract tip or fall freely. Upon entering the airflow field, the bracts will flip and separate under the influence of the airflow, thus separating the seeds trapped within the bracts. (2) When the initial orientation is stem down, the bracts will wrap around the seeds at the stem. Since the center of gravity of the bracts is close to the stem, resulting in a shorter moment arm, the torque generated by the airflow is relatively small. It is possible that the point of application of the airflow force coincides with the center of gravity of the bracts. Consequently, the bracts will only be influenced by the resultant force and will experience

an oblique acceleration and deviation. Therefore, a higher airflow velocity is required to flip the bracts with the stem-down orientation. (3) When the initial orientation is horizontal fall, the bracts will roll and flip under the influence of the airflow, facilitating seed separation.

Based on the analysis above, it is evident that the airflow field generated by the upper fan can cause the bracts to flip and achieve the desired effect of separating the bracts from the seeds. However, to enhance the effectiveness, it is necessary to moderately increase the outlet airspeed and reduce the initial orientation of stem-down bracts by adding a guiding slide plate (Figure 7).

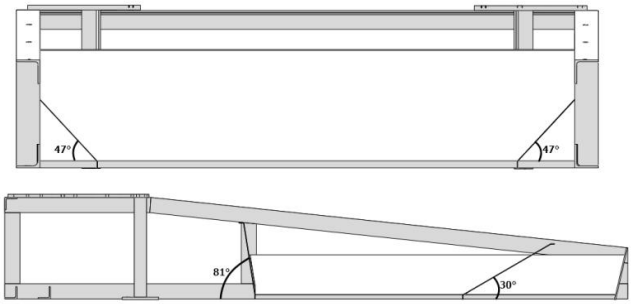

Figure 7. Diagram of the guide slide.

2.1.2. Design of Vibrating Screen Machine and Analysis of Material Forces on the Screen

The schematic diagram of the vibrating-screen mechanism is shown in Figure 8. It consists of a driving crank AB, a swing arm CD, a connecting rod BC, and parts such as the screen surface CE and slider E. The driving crank AB rotates and drives the connecting rod BC and swing arm CD to swing, thereby causing the screen surface CE to vibrate. Since the swing arm CD cannot perform rotational motion and is limited by the slider E, the motion trajectory of points on the screen surface CE differs before and after. The amplitude is larger in the vertical direction and smaller in the horizontal direction, while the conveying capacity in the horizontal direction remains the same.

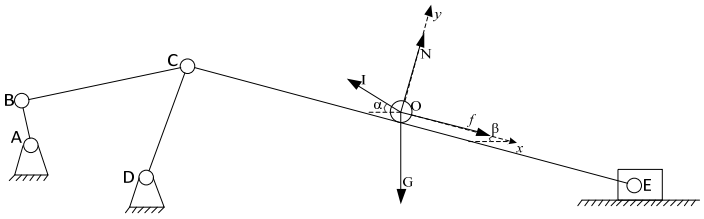

Figure 8. Structure diagram of vibrating screen and material force analysis.

The vibrating screen performs simple harmonic motion, and for the convenience of analysis, the lowest position of the screen is taken as the initial displacement and initial phase point of the screen motion [24]. The displacement equation of the screen is given by Equation (1):

$$x = A\cos(\omega t + \varphi) \tag{1}$$

Since the material moves along with the screen surface, the velocity and acceleration equations of the material on the screen can be obtained based on the displacement of the screen surface:

$$v = -A\omega\sin(\omega t + \varphi) \tag{2}$$

$$a = -A\omega^2\cos(\omega t + \varphi) \tag{3}$$

To facilitate the force analysis of the material on the screen surface, we select point O on the screen surface as the origin and establish a Cartesian coordinate system with the x-axis and y-axis parallel and perpendicular to the screen surface. Figure 5 illustrates the force situation on the material at point O.

The inertial force acting on the material is

$$I = -ma = Am\omega^2\cos(\omega t + \varphi) \tag{4}$$

$$I_x = I\cos\alpha = Am\omega^2\cos(\omega t + \varphi)\cos\alpha \tag{5}$$

$$I_y = I\sin\alpha = Am\omega^2\cos(\omega t + \varphi)\sin\alpha \tag{6}$$

In the equation, represents the inertial force acting on the material with its direction opposing the direction of material motion, thus being negative; represents the component of the inertial force in the x-direction; and represents the component of the inertial force in the y-direction.

The condition for the material to be thrown up is that the normal force acting on the material is zero, i.e.,

$$N = I_y - G\cos\beta = 0 \tag{7}$$

From Equation (7), we obtain

$$I_y = Gcos\beta \tag{8}$$

$$Am\omega^2\cos(\omega t + \varphi)sin\alpha = mgcos\beta \tag{9}$$

Because $0 \leq \cos(\omega t + \varphi) \leq 1$, therefore, $K = \frac{A\omega^2}{g} \geq \frac{\cos\beta}{\sin\alpha} = K_s K$ represents the vibration intensity of the vibrating screen, and K_s represents the critical value for the material to leap off the screen surface. Furthermore, the throwing index is defined as $D = \frac{K}{K_s}$; the material is thrown off the screen surface when $D > 1$. The larger D is, the higher the material is thrown, and vice versa.

3. Materials and Methods

3.1. CFD–EDEM Coupled Virtual Experiment

The centrifugal fan provides the airflow for the airflow field in the sorting room. Materials, such as bracts, corn, and short stalks, fall from the upper part of the sorting room and undergo initial screening through the action of the airflow. They then fall onto the vibrating screen, where the separation between seeds and bracts is achieved under the influence of the vibrating screen. The bracts and residual materials such as short stalks are expelled from the machine under the action of the draft bars [25]. Therefore, during the CFD–EDEM coupled simulation, the driving mechanism of the vibrating screen does not affect the sorting efficiency and can be omitted. Only the fan, draft bars, vibrating screen, and the outline of the sorting room need to be kept [26]. Through CFD–EDEM coupled simulation, the influence of the airflow field in the sorting room on the sorting process can be analyzed, and the structural design of the vibrating screen can be explored.

Before simulation, pre-processing of the model is necessary. This includes setting the physical and mechanical property parameters of the materials, selecting the collision model, and setting the coupling parameters, etc.

Based on the actual contact conditions of the materials, in EDEM, the contact mode is chosen as soft-sphere contact, and the contact model is selected as the Hertz–Mindlin no-slip contact model. The simulation time step should typically be approximately 20% of the Rayleigh time step. According to the actual requirements, the simulation step is set to 30% of the Rayleigh time step, and the total simulation duration is set to 4 s. In the coupled simulation, parameter settings for the fluid phase are also required, including boundary conditions and turbulent model selection. Since the measured wind speeds at the entrance of the recovery chamber do not exceed 20 m/s, the inlet velocity can be set to 20 m/s; the outlet is set as a pressure outlet, and since a low-pressure, medium-speed centrifugal fan is selected, the outlet pressure can be set to atmospheric pressure. The $k - \varepsilon$ turbulent model is chosen accordingly.

The physical and mechanical property parameters of the materials are shown in Tables 1–3.

Table 1. Material density.

Material	Density (kg/m^3)
corn	1197
short stalks	112
bracts	80

Table 2. Mechanical parameters of each material.

Material	Poisson's Ratio	Shear Modulus (GPa)
corn	0.4	0.127
short stalks	0.45	0.109
bracts	0.35	0.1
Steel (screen surface)	0.3	70

Table 3. Contact parameters between each material.

Material	Coefficient of Restitution for Collisions	Coefficient of Static Friction	Coefficient of Rolling Friction
corn–orn	0.32	0.55	0.01
corn–short stalks	0.26	0.34	0.01
corn–bracts	0.20	0.30	0.01
short stalks–short stalks	0.22	0.32	0.01
short stalks–bracts	0.19	0.47	0.01
bracts–bracts	0.25	0.76	0.01
corn–screen surface	0.54	0.41	0.01
short stalks–screen surface	0.29	0.33	0.01
bracts–screen surface	0.10	0.36	0.01

3.2. Field Experiment

In order to obtain the optimal combination of operating parameters for the upper-fan vibrating screen-type seed-recovery device, preliminary CFD–EDEM coupled simulation experiments were conducted on the vibrating screen orifice size, installation angle of the air distributor, and number of draft bars. Based on this, orthogonal experiments were performed on the driving-crank speed of the vibrating screen, fan speed, and operating speed to obtain the optimal combination of operating parameters for the upper-fan vibrating screen-type seed-recovery device.

Field experiments were conducted in Zhuangzhen Village, Laishui Town, Laishui County, Hebei Province. The maize variety used was Zhengdan 958, and the measured physical parameters of the maize plants are shown in Table 4.

Table 4. Physical parameters of corn plants.

Measurement Items	Row Spacing/cm	Plant Spacing/cm	Plant Height/cm	Ear Length/cm	Ear Diameter at the Base/cm	Ear Height/cm
Measurement value	60	27.5	275	26	62	123
	59	25.5	283	24	68	126
	59	29	243	25	65	118
	63	21	286	27	64	120
	58	27.5	268	26	60	129
	70	25	273	27	62	117
	68	22	274	27	58	115
	60	28	276	25	65	114
	62	24.5	291	26	64	120
	56	27	273	28	66	127
Average value	61.5	25.7	247.2	26.1	63.4	120.9

The main experimental equipment includes the prototype of the 4YJ-4 corn ear and stalk combine harvester, disassembly tools, several collection bags, stopwatches, measuring tapes, electronic balances, spare chain links, etc.

3.3. Test Indicators and Testing Methods

The field experimental methods and field investigations were conducted in accordance with GB5262 "General Rules for the Determination of Test Conditions for Agricultural Machinery", "Methods for Production Testing of Agricultural Machinery", and "Test Methods for Corn Harvesting Machinery". However, there are currently no specific regulations regarding the recovery performance of the corn seed-recovery device in the national standards. Therefore, the evaluation criteria for the corn seed-recovery rate and impurity content of corn seeds were determined based on the reference literature [27].

3.4. Design of Experiment

3.4.1. One-Factor Experiment

In the CFD–EDEM coupled simulation experiment, single-factor tests were conducted to determine the optimal structural parameters of the vibrating screen and the optimal installation angle of the air distributor. The screen aperture sizes of the vibrating screen were selected as 30 mm × 15 mm, 50 mm × 25 mm, and 70 mm × 35 mm. The number of draft bars was selected as 3, 5, and 7. The installation angle of the air distributor was selected as 0°, 7.5°, and 15°.

3.4.2. Orthogonal Experiment

Due to the influences of wind turbine speed, vibrating screen drive-crank speed, and operating speed on the performance of the corn grain-recovery device, an orthogonal experimental method was adopted to analyze the working performance of the device. Response surface analysis was conducted on the orthogonal experimental results to explore whether there are interaction effects among the factors and to determine the primary and secondary orders of the influencing factors as well as the optimal combination of operating parameters in order to provide a theoretical basis for achieving the optimal working state of the corn grain-recovery device. The levels of the orthogonal experimental factors are shown in Table 5.

Table 5. Levels of orthogonal test factors.

Level	Factors		
	Fan Speed(A)/r/min	Vibrating Screen Drive-Crank Speed(B)/r/min	Operating Speed(C)/km/h
1	800	200	3
2	1000	300	4
3	1200	400	5

The main function of the corn-recovery device is to recover the loss of kernels from the peeling device during detasseling and reduce grain loss. However, there are currently no specifications regarding the performance indicators for corn-recovery devices in the national standards. Therefore, based on the reference [10], the evaluation indicators for recovery performance are the corn-recovery rate and the corn-impurity rate. The corn-recovery rate is an important indicator and needs to be assessed during the experiment, while the corn-impurity rate is a general indicator that only requires visual observation for comparison and does not need to be the focus of assessment.

The calculation method for the corn-recovery rate is shown in Equation (10):

$$\delta_R = \frac{W_R}{W_A} \times 100\% \quad (10)$$

In the equation, W_R represents the mass of the corn collected in the recovery box in grams (g), and W_A represents the total mass of the corn fallen from the peeling device, also in grams (g).

Before the experiment, the centrifugal fan and the driven sprocket of the vibrating screen should be installed and tightened. Open the left and right covers and remove the blocking plate of the grain-collecting device. Start the machine to remove the grain-collecting device and any debris on the machine. The field experiments should be conducted according to the "Test Methods for Corn Harvesting Machinery" (GB/T21961-2008). Before the experiment, the working speed of the machine should be calibrated. Record the time required for the corn harvester to pass through a 15 m measuring area at a constant speed and mark the position of the walking control handle on the control panel when the walking speed is 3 Km/h, 4 Km/h, and 5 Km/h, respectively. The length of the test area is 15 m. Before the experiment, manually remove the lodged corn plants and weeds within the measuring area and then conduct the experiment according to the second rotation orthogonal table. After each experiment, observe the impurity content in the grain collecting box, weigh the collected grains, and clean the debris in the collecting bag for weighing. After weighing, start the machine and let it run without load for 1 min, remove any debris in the machine, manually clean other debris on the machine, and prepare for the next experiment. The experimental process is shown in Figure 9.

(**A**)

(**B**) (**C**)

Figure 9. Field experiment. (**A**) Field experiment process; (**B**) Collecting the recovered grains; (**C**) Collecting lost grains.

4. Experimental Results and Discussion

4.1. Analysis of CFD–EDEM Coupled Simulation Experiment

4.1.1. Virtual Experiment on Bract Motion Posture

The motion attitude of corn husks is shown in Figure 10. In the CFD–EDEM coupled simulation, the motion attitude of corn husks undergoes significant flipping changes due to the coupling effect of the airflow and vibrating screens. This significant motion attitude change demonstrates that the upper wind turbine vibrating screen-type grain-recovery device can effectively separate the grains embedded in the husks.

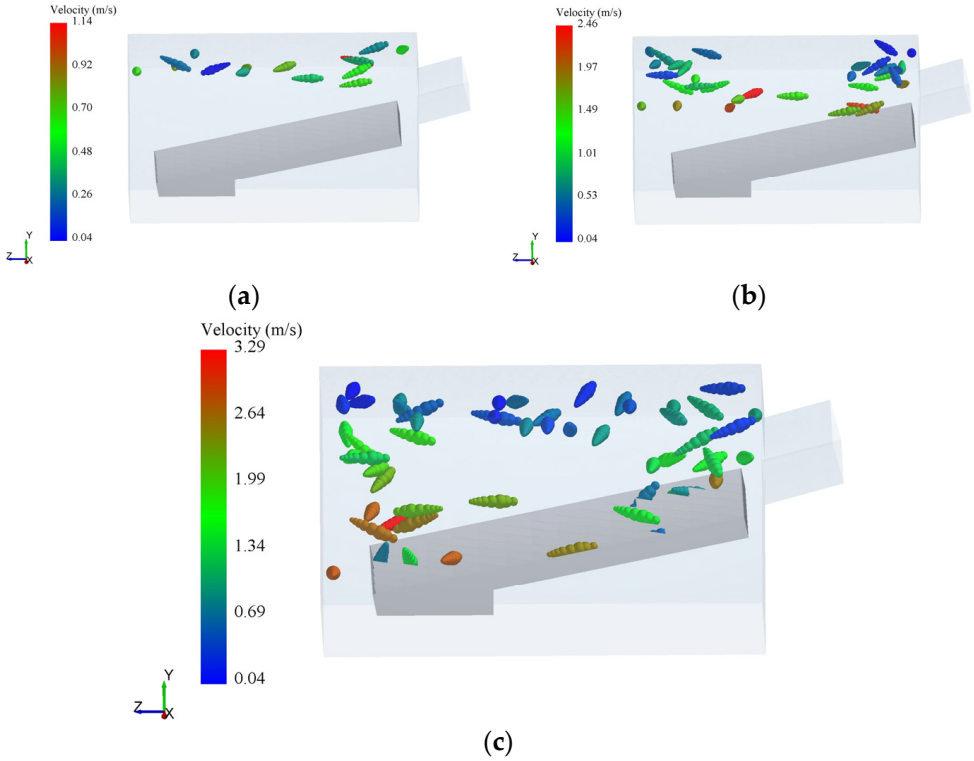

Figure 10. Motion posture of corn involucral leaves. (**a**) t = 0.1 s; (**b**) t = 0.2 s; (**c**) t = 0.3 s.

4.1.2. Virtual Experiment with Different Screen Aperture Sizes

The size of the vibrating screen sieve hole directly affects the types and quantities of materials that pass through the sieve. In this device, it mainly affects the recovery rate and impurity content of corn grains. In this single-factor experiment, the size of the vibrating screen sieve hole can be determined by analyzing the motion trajectory of corn grains and the quantity of short stems and corn grains that pass through the sieve.

Through the analysis in Figure 11, it is found that, during the process of corn grains falling from the husking device, the airflow exerts thrust on them, causing them to move backward. However, due to the fast floating speed of corn grains, the impact of the airflow on them is relatively small, and the distance they move backward is also relatively small. Therefore, we can separate the husks from the grains based on their different floating speeds. When the grains fall onto the sieve, they bounce back. According to Figure 8, the collision restitution coefficient between the corn grains and the sieve is large, resulting in a large bouncing amplitude. The size of the sieve determines the contact area between the grains and the sieve. Therefore, the smaller the sieve hole, the larger the contact area and the more severe the bouncing, which may cause some grains to bounce out of the machine, resulting in unnecessary losses. According to the analysis in Table 6, we found that, as the sieve hole size increases, the screening rate of corn grains also increases, but the screening rate of short stems also increases, leading to an increase in impurities mixed in with the recovered grains. Therefore, we believe that the optimal sieve hole size is 50 mm × 25 mm.

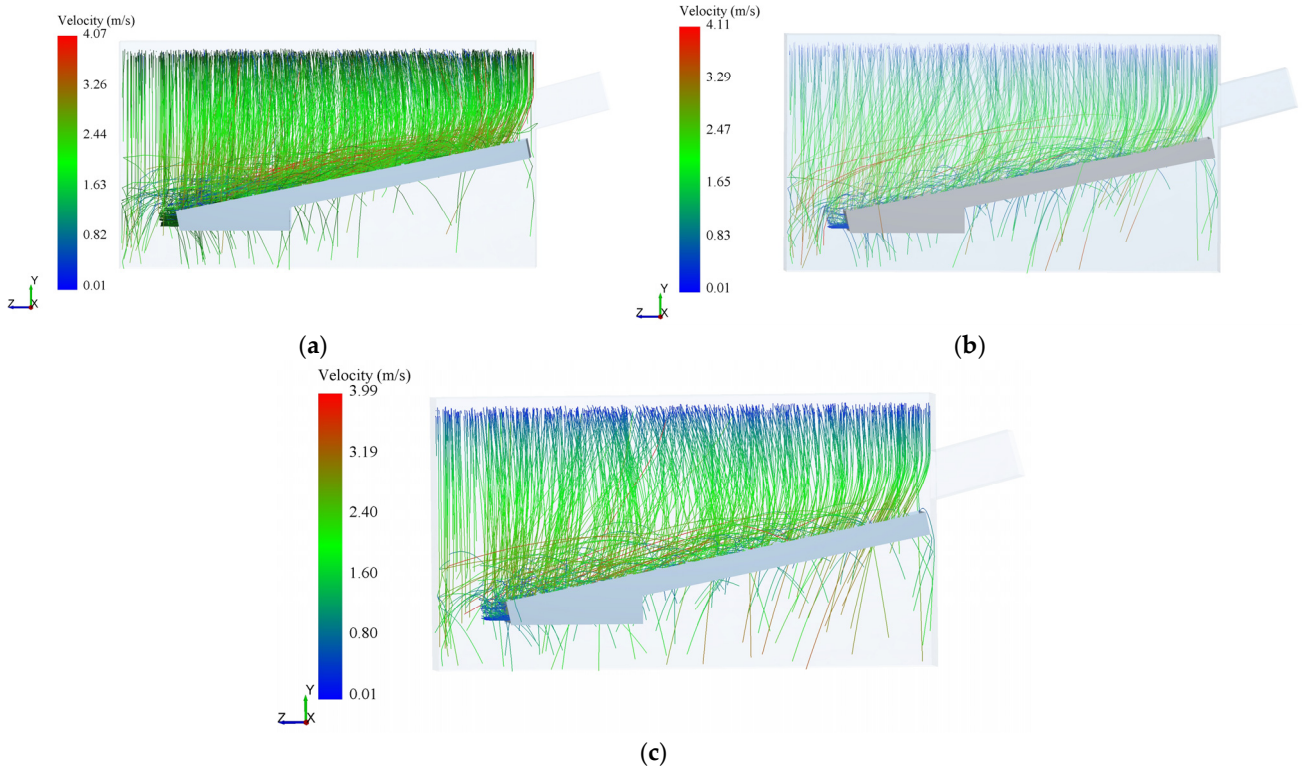

Figure 11. Trajectory of corn grain movement with different sieve hole sizes. (**a**) Grain Movement Trajectory in 70 mm × 35 mm Sieve Holes; (**b**) Grain Movement Trajectory in 50 mm × 25 mm Sieve Holes; (**c**) Grain Movement Trajectory in 30 mm × 15 mm Sieve Holes.

Table 6. Quantity of screened materials with different sieve hole sizes.

Sieve Hole Size	Number of Corn Seeds through the Sieve	Number of Short Stalks through Sieve
30 mm × 15 mm	2842	30
50 mm × 25 mm	3659	111
70 mm × 35 mm	3746	229

4.1.3. Virtual Experiment with Different Number of Finishing Passes

During the grain-recovery process, a large number of husks will fall onto the vibrating screen and participate in the cleaning process. The deflectors can effectively remove the larger-volume husks from the machine, thereby improving the efficiency of grain recovery. However, the installation of deflectors increases the collision area between the grains and the vibrating screen, resulting in the loss of corn grains. Therefore, the quantity of deflectors can be determined by analyzing the motion trajectory of the corn grains and husks as well as the quantity of corn grains and short stems that pass through the sieve.

According to Figure 12, when husks fall from the husking device, they are acted upon by gravity and airflow, causing them to move towards the rear of the recovery chamber. At the same time, under the influence of the airflow, the husks also undergo flipping, which facilitates the separation of the husks from the grains. After falling onto the sieve surface, the husks do not bounce back, but under the action of the vibrating screen and the deflectors, they move towards the rear of the sieve surface and are discharged out of the machine. By observing the motion trajectory of the husks under different quantities of deflectors, it was found that, with only three deflectors, the accumulation of husks on the sieve surface is severe, making it difficult to discharge them. As the quantity of deflectors increases, the accumulation of husks on the sieve surface decreases. Therefore, increasing the quantity of deflectors can effectively enhance the impurity removal capability of the grain-recovery device.

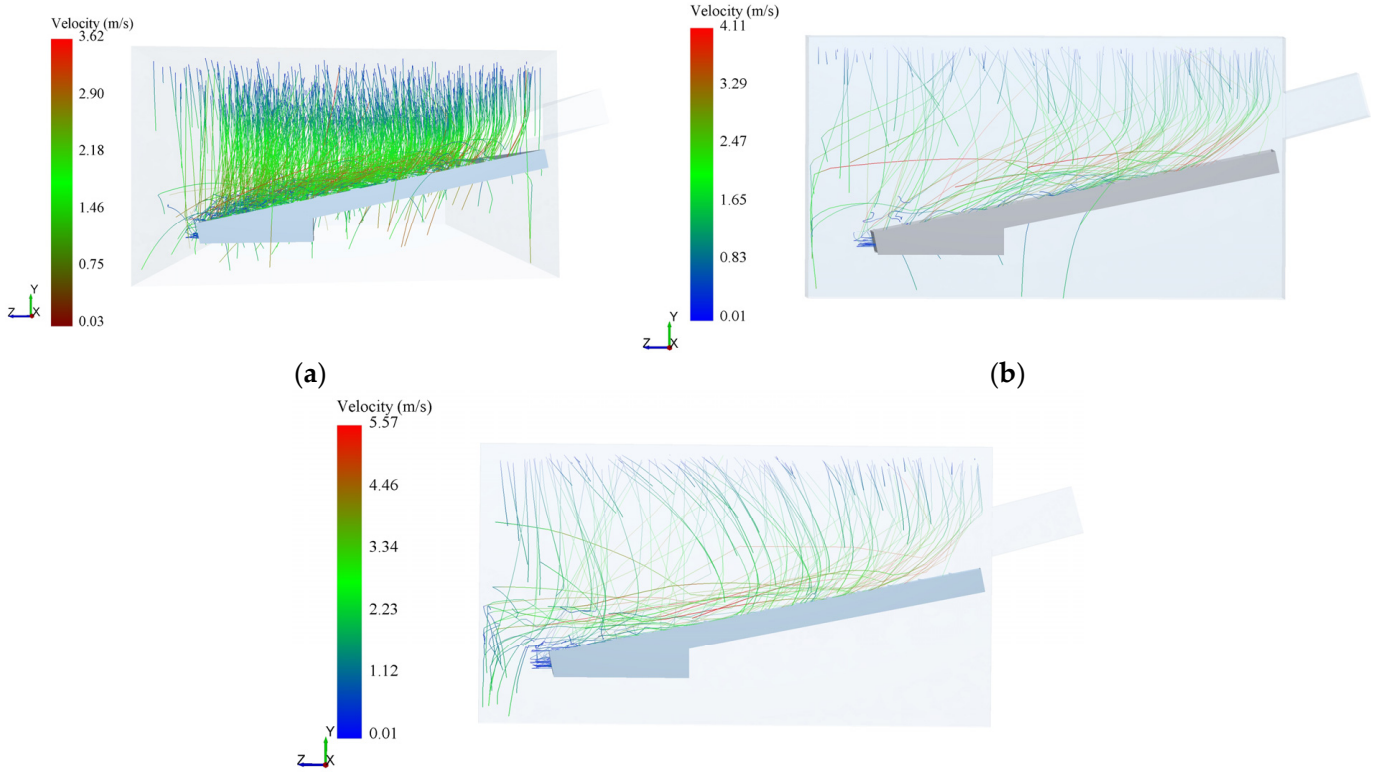

Figure 12. Motion trajectory of corn involucral leaves with different stripper bar numbers. (**a**) 3 draft-by-draft bract motion trajectories; (**b**) 5 draft-by-draft bract motion trajectories; (**c**) 7 draft-by-draft bract motion trajectories.

According to the analysis in Figure 13 and Table 7, under the same sieve hole size, different quantities of deflectors have little impact on the screening efficiency of lightweight impurities. This indicates that the designed deflectors mainly serve to remove husk residues and have a minimal effect on the removal of other lightweight impurities. However, when the quantity of deflectors reaches seven, the quantity of grains noticeably decreases. It was also observed that, with an increasing quantity of deflectors, the collision trajectory of the grains increases, and the motion trajectory becomes more chaotic. This is mainly because the husks face greater resistance between the deflectors, affecting their sliding towards the back of the sieve and, thereby, increasing the collisions between the grains and between the grains and husks. Therefore, an excessive quantity of deflectors can increase the collision loss of corn grains. In summary, it is considered that five deflectors are more suitable.

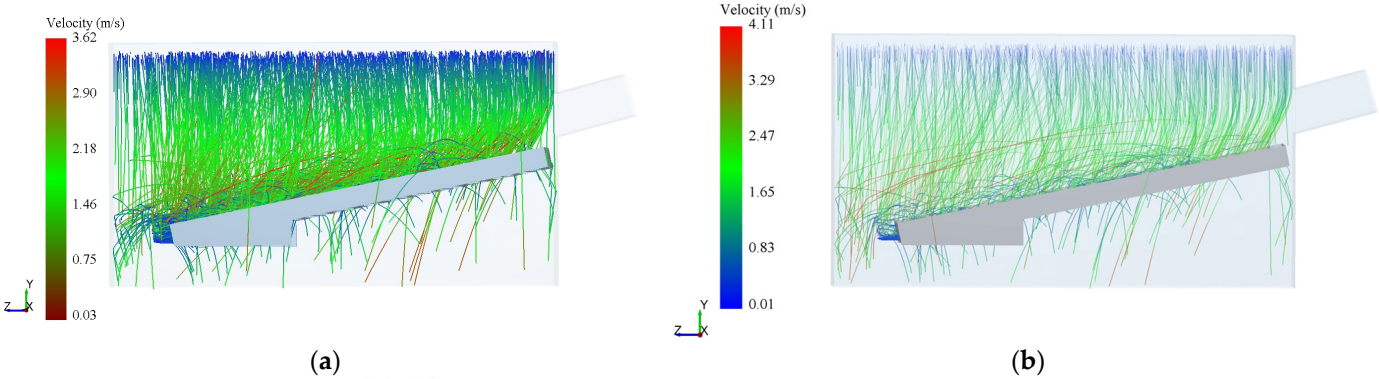

Figure 13. *Cont.*

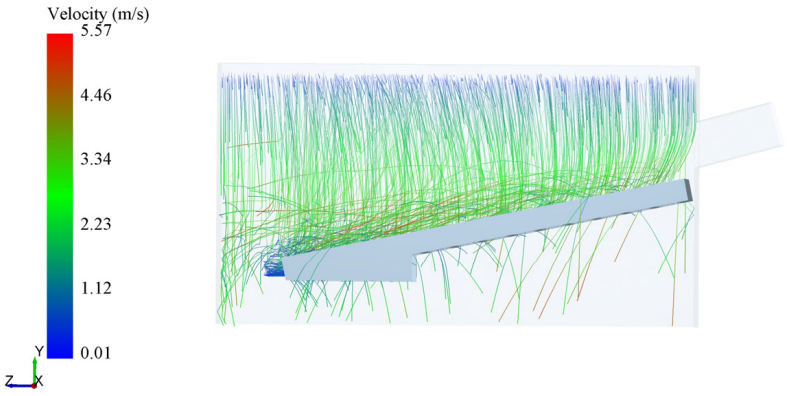

(**c**)

Figure 13. Motion trajectory of corn with different stripper bar numbers. (**a**) Trajectory of corn seed movement at 3 strips-by-strip; (**b**) Trajectory of corn kernel movement at 5 draft-by-strip; (**c**) Trajectory of corn seed movement at 7 draft-by-strip.

Table 7. Quantity of screened materials with different stripper bar numbers.

Number of Draft-by-Stalk	Number of Corn Seeds through the Sieve	Number of Short Stalks through Sieve
3	3689	88
5	3659	111
7	3519	107

4.2. Orthogonal Experiment

The orthogonal experimental design and experimental results are shown in Table 8.

Table 8. Orthogonal test scheme and test results.

Serial Number	Fan Speed (rpm)	Vibrating Screen Rotating-Shaft Speed (rpm)	Operating Speed (km/h)	Grain-Recovery Rate (%)
1	1200	400	4	74.51
2	1000	400	5	81.39
3	1000	400	3	71.34
4	800	400	4	73.76
5	1200	300	3	76.04
6	1200	300	5	70.08
7	1000	300	4	83.06
8	1000	300	4	84.99
9	1000	300	4	85.58
10	800	300	3	75.70
11	800	300	5	69.08
12	1200	200	4	70.60
13	1000	200	3	76.47
14	1000	200	5	78.70
15	800	200	4	68.66

Results and Analysis

The experimental results were subjected to multivariate regression fitting analysis and analysis of variance (ANOVA) using Design-Expert software with F-tests conducted on the experimental factors and the regression model. The results are shown in Table 9.

In Table 9, A means fan speed, B means vibrating screen drive-crank speed, and C means operating speed.

Table 9. Results of variance analysis.

Source of Variance	Sum of Squares of Bias Variance	Degrees of Freedom	Mean Square	F-Value	*p*-Value
A	5.3956125	1	5.395613	1.176936	0.327496
B	2.0301125	1	2.030113	0.442825	0.535224
C	52.02	1	52.02	11.34703	0.019921
AB	0.354025	1	0.354025	0.077223	0.792221
AC	37.6996	1	37.6996	8.223349	0.035091
BC	0.1089	1	0.1089	0.023754	0.88354
A^2	65.30041603	1	65.30042	14.24387	0.012968
B^2	263.9781083	1	263.9781	57.58109	0.000631
C^2	41.75707756	1	41.75708	9.108399	0.029483
Model	431.0940017	9	47.89933	10.4482	0.009386
Residuals	22.92229167	5	4.584458		
Misfit	19.447825	3	6.482608	3.73157	0.218517
Error	3.474466667	2	1.737233		
Total	454.0162933	14			

According to the analysis of variance table, it can be observed that the impact of the operating speed in the linear term is the most significant, while the *p*-values of the quadratic terms for wind turbine speed, vibrating screen speed, and operating speed are all less than 0.05. In addition, the *p*-value of the quadratic term for vibrating screen speed is less than 0.001, indicating that the quadratic terms of all factors have a significant impact on the grain-recovery rate with vibrating screen speed having an extremely significant impact on the grain-recovery rate. Furthermore, the *p*-value of the AC interaction term is less than 0.05, indicating that this interaction term also has a significant impact on the grain-recovery rate. The *p*-value of the established model is less than 0.05, and the lack-of-fit term has a *p*-value of 0.218517, indicating that the established model fits accurately without distortion. After removing the non-significant terms, the obtained fitted equation is:

$$R = 84.5433 - 2.55 \times C + 3.07 \times A \times C - 4.2054 \times A^2 - 8.4554 \times B^2 - 3.3629 \times C^2 \quad (11)$$

After obtaining the fitted equation, to analyze the impact of each factor on the grain-recovery rate, single-factor analysis and response surface analysis were conducted on each factor and interaction term using Design-Expert, and the results are shown in Figures 14 and 15.

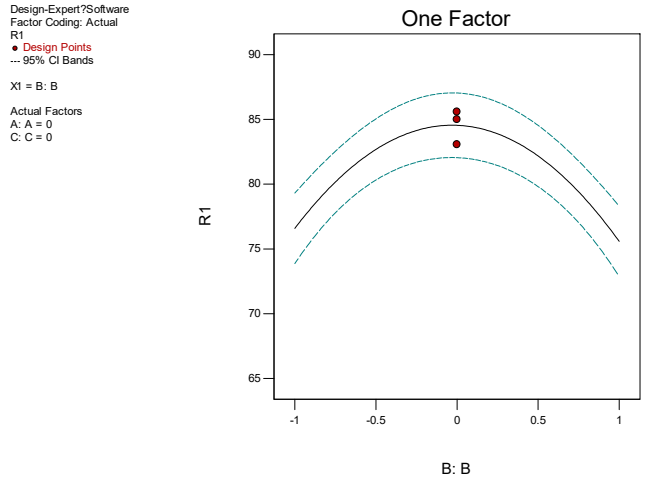

Figure 14. Single-factor analysis.

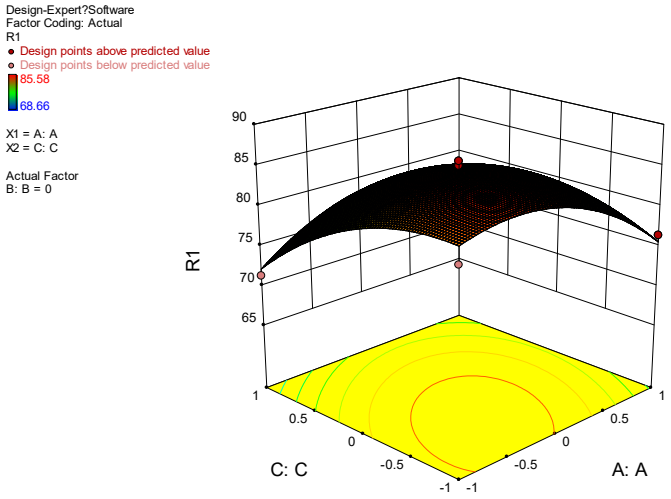

Figure 15. Response surface analysis.

Since A and C are interaction terms, response surface analysis needs to be used to consider their effects on the results. At the same time, the influence of B can be studied through single-factor analysis. Single-factor analysis shows that the grain-recovery rate is quadratically correlated with the rotational speed of the vibrating screen crank. When the speed is too low, the mixture cannot be effectively thrown up, resulting in the inability to separate the grains from the impurities, which leads to losses. When the speed is too high, the grains are bounced up and fall on the screen surface and are then carried out by the bracts, also causing losses. Response surface analysis indicates that the grain-recovery rate is negatively correlated with the operating speed and quadratically correlated with the fan speed. With a faster operating speed, more materials need to be classified in the same-sized recovery chamber, increasing the difficulty and causing the grains to be discharged without separation. If the fan speed is too low, the bracts cannot fully flip and separate from the grains, while a speed that is too high will blow the mixture out before it can separate from the impurities. Overall, the slope of the response surface is very steep, indicating that the interaction between the operating speed and fan speed is highly significant.

By using the Design-Expert optimization method with the optimization goal of maximizing the grain recovery rate, the optimal solutions for the fan speed, vibration screen speed, and operating speed are obtained as shown in Figure 16.

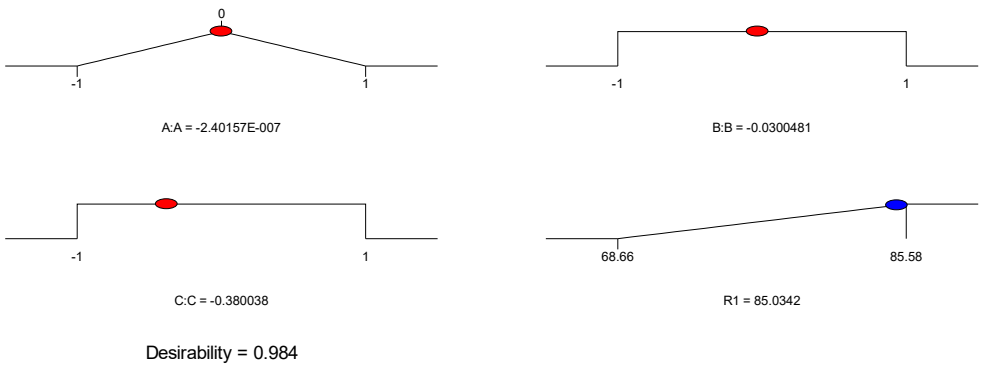

Figure 16. Target optimization.

The optimal solutions given by Design-Expert are in coded form and should be converted into actual numerical values. The optimal values for A (fan speed) and B (vibrating screen crank speed) in the coding are very close to zero. After converting them into actual values, the errors with the experimental levels are extremely small. Therefore, it can be considered that their optimal solutions in the coding are at the zero level. Based on

the above analysis, the optimal solution is obtained as follows: fan speed of 1000 r/min, vibrating screen crank speed of 300 r/min, operating speed of 3.62 km/h, and grain-recovery rate of approximately 85%.

5. Discussion

Through the coupled CFD–EDEM experiment, it is found that corn bracts can flip under the action of airflow and vibrating screens, which proves that the upper-fan vibrating screen-type grain-recovery device can effectively separate the grains trapped in the bracts.

Through virtual simulation single-factor experiments, it is found that, when the sieve holes of the vibrating screen are too large, more impurities such as short stalks can pass through, resulting in an increased impurity content in the corn grains. When the sieve holes are too small, the collision area between the corn grains and the vibrating screen increases, causing increased losses due to collisions and a decrease in the grain-recovery rate. Therefore, it is determined through single-factor experiments that the size of the sieve holes in the vibrating screen should be 50 mm × 25 mm. Having too few rows on the vibrating screen will weaken its ability to remove impurities, making it difficult to discharge the corn bracts from the vibrating screen, thus reducing the cleaning efficiency of the grain-recovery device and causing a decrease in the grain-recovery rate. On the other hand, having too many rows will increase the collision area between the corn grains and the vibrating screen and result in increased losses due to collisions, also leading to a decrease in the grain-recovery rate. Therefore, it is determined through single-factor experiments that the number of rows should be set to five.

Through the analysis of the orthogonal experimental results of the grain-recovery device, it is found that the operating efficiency of the device is influenced by the cleaning fan speed, vibrating screen crank speed, and operating speed. The effects of each factor on the grain-recovery rate are determined through variance analysis, and a fitted equation after eliminating insignificant items is obtained. Then, using the target optimization method with the optimal goal of maximizing the grain-recovery rate, the optimal working parameters are obtained as follows: fan speed of 1000 r/min, vibrating screen crank speed of 300 r/min, and operating speed of 3.62 km/h. At this setting, the grain-recovery rate should be approximately 85%.

6. Conclusions

In this paper, aiming at the problem of corn grain loss caused by the peeling device during the simultaneous harvesting of corn ears and stalks, a top-mounted fan vibrating screen grain-recovery device is designed, and the working principle of the grain-recovery device is specifically described. CFD–EDEM coupled simulation experiments were conducted on the grain-recovery device to simulate the motion trajectories of corn bracts and grains under different vibrating-screen structures, and the number of passing materials was statistically analyzed. Finally, through field experiments, the impact of fan speed, vibrating screen crank speed, and operating speed on the working performance of the grain-recovery device was investigated. The following conclusions were drawn:

(1) The force analysis of corn bracts with different initial attitudes in the airflow field was conducted, and their motion attitudes were simulated and analyzed in the CFD–EDEM coupled simulation. It was proven that the top-mounted fan vibrating screen grain-recovery device can effectively cause the flipping of corn bracts and separate the corn grains trapped within them.

(2) Through CFD–EDEM coupled simulation, the structural parameters of the vibrating screen were optimized. By analyzing the motion trajectories of the corn grains and the number of passing materials under different sieve hole sizes, the optimal sieve hole size for the vibrating screen was determined to be 50 mm × 25 mm. By analyzing the motion trajectories of the corn bracts and grains as well as the number of passing materials under different numbers of rows, the optimal number of rows was determined to be five.

(3) Through field experiments on the grain-recovery device, the optimal working parameters of the top-mounted fan vibrating screen grain-recovery device were determined to be a fan speed of 1000 r/min, vibrating screen crank speed of 300 r/min, and operating speed of 3.62 km/h. At this setting, the grain-recovery rate is approximately 85%.

(4) The fan speed, vibration screen speed, and operating speed are important factors that determine the corn kernel-recovery rate. The selected operating speed in this experiment was relatively low. In order to improve the operating efficiency of the corn combine harvester, hydraulic motor drive can be used, and further research can be conducted using intelligent control methods based on response equations.

Author Contributions: Conceptualization, Y.G. and F.X.; methodology, Y.L.; software, Y.L.; validation, Y.G.; formal analysis, Y.Y.; investigation, Y.L.; resources, Y.Y. and F.X.; data curation, Y.L. and Y.G.; writing—original draft preparation, Y.L.; writing—review and editing, Y.G.; visualization, Y.Y.; supervision, Y.G.; project administration, F.X.; funding acquisition, F.X.; All authors have read and agreed to the published version of the manuscript.

Funding: This work was mainly supported by the Natural Science Foundation of Shandong Province, ZR2020ME136; Shandong Province Key R&D Program (Major Science and Technology Innovation Project)-Research and Development of High-Efficiency Production Equipment for Specialty Vegetables-2022CXGC010612; Shandong Province Higher Education Institutions Young Innovation Team Talent Introduction Program.

Institutional Review Board Statement: Not applicable.

Data Availability Statement: Data are contained within the article. The data presented in this study can be requested from the authors.

Conflicts of Interest: The authors declare no conflict of interest.

References

1. Cui, A.; Zhang, J.; Zhang, H.; Shan, H.; Chen, W. Preliminary Exploration on Current Situation and Development of Maize Production in China. *J. Agric. Sci. Technol.* **2020**, *22*, 10–19.
2. Lu, D. *Research on Optimization of Maize Production Cost in China*; Chinese Academy of Agricultural Sciences Dissertation: Beijing, China, 2018.
3. John Deer. X9 Technology Packages. Available online: http://www.deere.com/en/harvesting/x-series-combines/technology-packages/ (accessed on 2 April 2021).
4. Shinners, K.J.; Binversie, B.N. Fractional yield and moisture of corn stover Biomass produced in the Northern US Corn Belt. *Biomass Bioenergy* **2007**, *31*, 101–106. [CrossRef]
5. Igathinathane, C.; Womac, A.R.; Sokhansanj, S. Corn stalk orientation effect on mechanical cutting. *Biosyst. Eng.* **2010**, *107*, 97–106. [CrossRef]
6. Wang, J.; Li, Y.; Ma, Z.; Hu, B.; Yu, S. Structural Characteristics and Development Trend of Key Equipment of Corn Harvesting Machinery. *J. Agric. Mech. Res.* **2019**, *41*, 1–8.
7. Xu, Y.; Tao, P. Study on Influencing Factors of Mechanical Harvest Loss of Summer Maize in Hebei Province—Based on Xinji City. *Anhui Agric. Sci.* **2020**, *48*, 226–228+231.
8. Mu, P. *Research on High Net and Low Loss Cleaning Screen of Corn Grain Harvester*; Jilin University: Changchun, China, 2020.
9. Cui, T.; Fan, C.; Zhang, D.; Yang, L.; Li, Y.; Zhao, H. Research Progress of Maize Mechanized Harvesting Technology. *Trans. Chin. Soc. Agric. Mach.* **2019**, *50*, 1–13.
10. Wang, G. *Design and Research for the Grain Recovery Device of Corn Harvester*; Chinese Academy of Agricultural Mechanization Sciences: Beijing, China, 2013.
11. Zhou, X.; Liu, H.; Zeng, C. Design of Integrated Maize Harvester's Ear Leaf Cutter and Grain Recovery Wind Selection Device. *Agric. Dev. Equip.* **2017**, *49*, 67–68.
12. Jing, Y. Development and Application of a Grain Recycling Device for Corn Combine Harvesters. *Agric. Dev. Equip.* **2017**, *23*, 62–63.
13. Shen, H. *Research and Development of Hydraulic Control System for Corn Combine Harvester*; University of Jinan: Jinan, China, 2019.
14. Miu, P.I. Mathematical model of threshing process in an axial unit with tangential feeding. In Proceedings of the AIC 2002 Meeting CSAE, Saskatoon, SK, Canada, 14–17 July 2012; pp. 212–219.
15. Tang, H.; Xu, C.; Zhao, J.; Wang, J. Stripping mechanism and loss characteristics of a stripping-prior-to-cutting header for rice harvesting based on CFD-DEM simulations and bench experiments. *Biosyst. Eng.* **2023**, *229*, 116–136. [CrossRef]
16. Tang, H.; Xu, F.D.; Xu, C.S.; Zhao, J.L.; Wang, Y.J. The influence of a seed drop tube of the inside-filling air-blowing precision seed-metering device on seeding quality. *Comput. Electron. Agric.* **2023**, *204*, 107555. [CrossRef]

17. Tang, H.; Xu, C.S.; Xu, W.L.; Xu, Y.N.; Xiang, Y.S.; Wang, J.W. Method of straw ditch buried returning, development of supporting machine and analysis of influencing factor. *Front. Plant Sci.* **2022**, *13*, 967838. [CrossRef]
18. Tang, H.; Xu, C.S.; Wang, Z.M.; Wang, Q.; Wang, J.W. Optimized design, monitoring system development and experiment for a long-belt finger-clip precision corn seed metering device. *Front. Plant Sci.* **2022**, *13*, 814747. [CrossRef]
19. Wang, Z.; Che, D.; Bai, X.; Hu, H. Improvement and Experiment of Cleaning Loss Rate Monitoring Device for Corn Combine Harvester. *Trans. Chin. Soc. Agric. Mach.* **2018**, *49*, 100–108.
20. Li, H.; Zhang, M.; Yin, W.; Li, Y. Optimization of Airflow Field on Air-and-screen Cleaning Device Based on CFD. *Trans. Chin. Soc. Agric. Mach.* **2013**, *44*, 12–16.
21. Wang, L.; Jiao, Z.; Zhao, G. Simulation Analysis of Centrifugal Fan in Air Screen Type Cleaning Device. *Agric. Equip. Veh. Eng.* **2017**, *55*, 10–14.
22. Li, Q.; Jin, C.; Teng, Y.; Ning, X.; Liu, P. Experimental Optimization of Main Parameters of Multi—Channel Centrifugal Fan with Double Outlet. *J. Agric. Mech. Res.* **2021**, *43*, 190–196.
23. Du, Z.; Hu, Y.; Qiu, S.; Chen, Y. Optimization Design and Experiment of Air Duct on Spray Cooling Fan. *Trans. Chin. Soc. Agric. Mach.* **2020**, *51*, 118–125+151.
24. Zhang, F.; Wei, X.; Chen, K.; Yuan, S.; Wang, Y.; Chen, H. Internal Vortex Characteristics of Side Channel Pump with Convex Blade. *Trans. Chin. Soc. Agric. Mach.* **2020**, *51*, 115–122.
25. Hao, F.; Chen, Z.; Zhang, Z.; Han, Y.; Yu, P.; Han, Z. Design and Experiment of Corn Stalk Combined Harvesting Header Stalk Chopping Conveyor. *Trans. Chin. Soc. Agric. Mach.* **2019**, *50*, 67–72.
26. Wang, G.; Cao, H.; Han, Z.; Hao, F.; Wu, H.; Su, T. Analysis of Crank Connected Vibrating—Sieve Device in Corn Harvester. *J. Agric. Mech. Res.* **2014**, *36*, 65–68+72.
27. Wang, G.; Cao, H.; Han, Z.; Wu, H.; Feng, X.; Hao, F. Analysis and Prospects of the Corn Kernel Recovery Unit of Corn Harvester. *J. Agric. Mech. Res.* **2013**, *35*, 221–224.